M. Aronniemi, J. Sainio, J. Lahtinen, XPS study on the correlation between chemical state and oxygen-sensing properties of an iron oxide thin film, Helsinki University of Technology, Publications in Engineering Physics A, Report TKK-F-A851 (2007). Applied Surface Science, accepted for publication (2007).

XPS study on the correlation between chemical state and oxygen-sensing properties of an iron oxide thin film

M. Aronniemi *, J. Sainio J. Lahtinen

Laboratory of Physics, Helsinki University of Technology, P.O.Box 1100, FI-02015 TKK, Finland

Abstract

We have studied the correlation between the chemical state and the oxygen sensing properties of an iron oxide thin film using a setup that allows simultaneous sensor resistance measurements and XPS data acquisition. The gas exposures were performed at the highest operating pressure of the XPS spectrometer at a controlled sample temperature which allows direct comparison between the sensor response and the chemical state of the surface. The iron oxide film was modified by a sequence of argon ion sputtering steps and the induced changes in the chemical state, resistance, and sensitivity to oxygen were investigated. The sputtering was found to reduce the iron from the Fe^{3+} to the Fe^{2+} state and to decrease the sensor resistance. The measured sensitivity to oxygen first increased by a factor of two but then collapsed to its original level. The mechanism for oxygen sensing was found to be filling of the oxygen vacancies in the lattice. The effect of the sputtering on the resistance and sensitivity could be explained first with an increase in the density of oxygen vacancies and then, as the iron became more reduced, with an increase in the p-type conductivity.

Key words: XPS, iron oxide, thin film, gas sensor, oxygen, factor analysis, chemical state

1 Introduction

Semiconductive metal oxides are widely studied in order to develop inexpensive and simple gas sensors. Their applications are typically in monitoring

* Corresponding author.
Email address: Mikko.Aronniemi@tkk.fi (M. Aronniemi).

combustible or toxic gases, such as O_2, CO, H_2, NO_2, and CH_4. The metal oxide functions as a gas-sensitive material by changing its resistance due to exposure to oxidizing or reducing gases. Typically, the target gas affects the sensor resistance by i) changing the density of adsorbed oxygen generating localized surface states that trap conduction band electrons and/or ii) changing the concentration of oxygen vacancies acting as donors [1].

The sensitivity of a given oxide to various target gases is affected by its chemical and structural properties. In order to understand the sensing mechanism in detail, one should find the relation between the chemical changes on the surface and the electrical response, typically resistance change. XPS (x-ray photoelectron spectroscopy) is a widely used tool for the chemical analysis of surfaces and it has been applied in some extent also to gas sensor studies [2–9]. Maffeïs et al. [4] studied a nanocrystalline SnO_2 gas sensor with XPS and reported on the band bending caused by gas exposure; they also correlated the band bending with changes in bulk resistance [5]. Kawabe et al. [6] investigated different oxygen species on the surface of a SnO_2 thin film after various treatments, such as argon ion sputtering and oxygen exposure at elevated temperatures.

The generic difficulty in the XPS analysis of gas sensors stems from the limited operating pressure of a typical XPS system combined with the high operating temperature of the sensor. In order to mimic the realistic operation conditions, the gas exposures are typically conducted at an elevated temperature at the atmospheric pressure. When the chamber is then evacuated to UHV for the XPS measurement, the surface chemical state may change due to desorption or diffusion, in particular if the sensor is kept at the operating temperature. Consequently, the recorded photoelectron spectra may not be representative for the sensor surface during the actual sensing. In addition, with a standard XPS system it is seldom possible to monitor the sample resistance inside the chamber.

In the present work, we have used for the first time to our knowledge a setup which allows simultaneous gas exposure, resistance measurement, temperature control, and XPS data acquisition. By performing the gas exposures at the highest operating pressure of the spectrometer (4×10^{-7} mbar), the XPS spectra could be recorded during the exposure, and the observed chemical changes can be directly correlated with the changes in the electrical and sensing properties.

The gas sensor studied here is based on a thin film of iron oxide in the α-Fe_2O_3 (hematite) phase. The sensor surface was modified by argon ion sputtering and the changes induced in the chemical state, resistance, and oxygen-sensitivity were investigated. Similar to the most popular sensor material SnO_2, Fe_2O_3 is an n-type semiconductor with oxygen vacancies acting as donors [10–12]. Due

to a higher sputtering yield of oxygen compared to iron, argon ion sputtering is expected to extract oxygen from the oxide which can be detected with XPS. This surface modification should cause significant changes in the sensing behavior of the iron oxide film. Quantitative analysis of the chemical state of iron was carried out using factor analysis, the applicability of which to XPS data analysis has been demonstrated in Ref. [13].

2 Experimental

2.1 Sample

The sensor sample was prepared on a 4×4 mm^2 glass substrate. Before the film deposition, platinum electrodes for resistance measurement and temperature control were evaporated on the top and bottom side of the substrate, respectively. The electrode structure for resistance measurement consisted of 22 pairs of interdigital electrodes having a width of 20 μm, length of ~ 2 mm, and spacing of 20 μm. The iron oxide film was grown with ALD (atomic layer deposition) [14,15] using $FeCl_3$ and H_2O as precursors. The growth procedure consisted of 5000 reaction cycles at 500 °C. Characterization of the film has been reported elsewhere [16]. In brief, SEM (scanning electron microscope) and AFM (atomic force microscope) measurements indicated that the film had grown mainly on the glass substrate leaving the platinum electrodes almost uncovered. The film contained grains whose lateral diameter was on the order of 200 nm and height between 50 and 200 nm. According to XRD (x-ray diffraction), the iron oxide was in the α-Fe_2O_3 (hematite) phase. Electric conductivity showed an activation energy of about 0.3 eV and almost Ohmic I–V dependency.

2.2 Instrumentation

The sensor sample was mounted on a custom-made sample holder in the analysis chamber of the XPS system. The base pressure in the chamber was 4×10^{-9} mbar and the gas exposures were made at 4×10^{-7} mbar which was the maximum operating pressure of the spectrometer. The oxygen (99.999 %, AGA) used in the exposures was dosed with a manual leak valve. The sample was sputtered with a differentially pumped ion gun operated at 4 kV and ~ 60 nA/cm^2. The XPS spectra were collected with a Surface Science Instruments SSX-100 ESCA spectrometer using monochromatic Al K_α x-rays (1486.6 eV) and an electrostatic hemispherical analyzer. Core-level spectra were recorded with a pass energy of 55 eV and an x-ray spot size of 600 μm, which gave for

the Au $4f_{7/2}$ peak a FWHM of 0.95 eV. The binding energy step size was 0.1 or 0.05 eV.

The sensor resistance was measured and its temperature controlled with National Instruments Field Point modules and a LabVIEW-based user interface including a PID control for the sensor temperature. The sampling period was 1.5 s. The bias voltage source was set to provide a constant voltage of 0.6 V over the sensor, irrespective of the sensor resistance.

2.3 Treatment

In order to study the correlation between the chemical state and gas-sensing properties of the iron oxide film, the sensor sample was subjected to a sequence of 17 sputtering and oxygen exposure steps. Each step consisted of

- sputtering with 4-keV argon ions
- recording XPS spectra of Fe 2p (700–745 eV), O 1s (525–540 eV), Pt 4f (68–85 eV), and a survey scan (0–1100 eV)
- recording a 50-min resistance response of the sensor to oxygen at 4×10^{-7} mbar
- recording the same XPS spectra under the oxygen exposure

The sensor resistance was monitored continuously but the bias voltage was minimized when recording the spectra in order to avoid broadening of the peaks. The temperature of the sensor was held at 300 °C throughout each step. The cumulative sputtering time corresponding to each step is indicated in Table 1.

Table 1
Cumulative sputtering time as a function of the step index.

Step index	1	2	3	4	5	6	7	8	9
Time (s)	10	30	90	150	270	470	970	1370	1970
Step index	10	11	12	13	14	15	16	17	
Time (s)	2570	3170	4070	5270	7670	10070	17270	25670	

2.4 XPS data analysis

The main objective of the XPS data analysis was to determine quantitatively the relative amounts of the two chemical states, Fe^{2+} and Fe^{3+}, in each recorded spectrum. Because factor analysis was used to resolve the chemical

states, it was first necessary to remove shifts, other than chemical, from the Fe 2p spectra. The shifting of the peaks results mainly from band bending, i.e. variation in the Fermi level position, caused by changes in the density of localized surface states as a result of different sample treatments [1,4]. In order to separate the chemical shift from the band bending, it was assumed that neither of them affects the Pt 4f peaks and that there is no chemical shift in the O 1s main peak, i.e., oxygen atoms bound to Fe^{2+} and Fe^{3+} have equal binding energies.

First, the Pt 4f spectra were fitted with two mixed Gaussian–Lorentzian peaks with an exponential tail [17,18]. The maximum of the Pt $4f_{7/2}$ peak varied around 71.3 eV. This was chosen as the binding energy reference, i.e. all spectra of each step were corrected to set the Pt $4f_{7/2}$ peak to 71.3 eV. Secondly, the band bending was determined as the shift of the O 1s main peak corresponding to lattice oxygen; 530.3 eV was chosen (arbitrarily) as the position of zero band bending. Because the spectrum was broadened on the high binding energy side, two Gaussian components were fitted to the data with the separation fixed to 1.5 eV (see discussion below). Finally, the band bending was removed from the Fe 2p spectra, leaving only the chemical shift due to variation in the proportions of the Fe^{2+} and Fe^{3+} states.

To remove the contribution of inelastic photoelectrons from the Fe 2p spectra, the universal Tougaard background [19] with $C = 1643$ eV^2 was employed. Before the background subtraction, the spectra were corrected for the energy response of the analyzer by assuming that the recorded intensity I depends on the electron kinetic energy as $I \propto E_{\mathrm{kin}}^{-0.7}$. In addition, a slope was subtracted to remove the background of the lower binding energy peaks, mainly O 1s. The Tougaard B parameter was determined using a range of 690–820 eV of the survey spectrum. The obtained values were around 3400 eV^2, thus being in accordance with typical bulk values. To obtain equal weights in the factor analysis, the background-subtracted spectra were normalized to unit area.

The factor analysis was performed as described in Ref. [13]: Instead of using reference spectra, a narrow Gaussian peak (FWHM = 0.1 eV) was taken as the test component and its position was varied on the binding energy scale in order to find acceptable representations for the chemical states.

3 Results and discussion

3.1 Chemical states of iron and oxygen

The sputtering and oxygen exposure sequence consisted of 17 steps. In each step, the photoelectron spectra were collected twice, before and during the oxygen exposure. A few examples of the recorded Fe 2p and O 1s spectra are shown in Fig. 1.

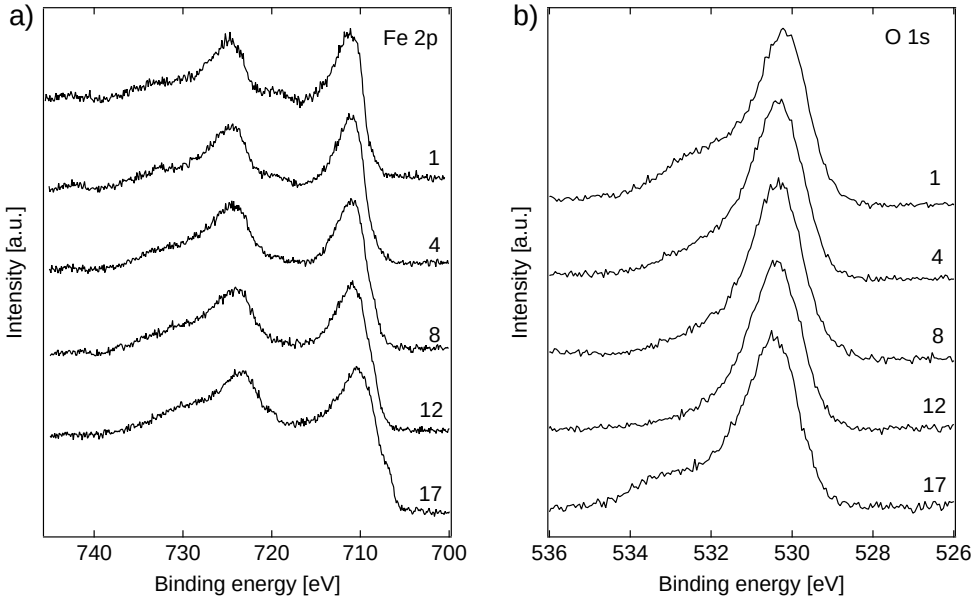

Fig. 1. Examples of the recorded Fe 2p (a) and O 1s spectra (b). The index of the step is indicated beside each spectrum, all recorded before the oxygen exposure.

In the factor analysis of the Fe 2p spectra, the indicator function [20] minimized at 3 suggesting that the data contains three components, most likely Fe^0, Fe^{2+}, and Fe^{3+}. However, because the metallic state seemed to be present only in the last step, the analysis was performed with two components. The obtained components as well as the reproduction of one of the recorded spectra are shown in Fig. 2a. The agreement between the reproduction and the data is good and the shape of the components is well in accordance with those reported in the literature for Fe^{2+} and Fe^{3+} [17,21–23]. The agreement between the reproduction and the data was practically equally good for all the recorded spectra.

As a result of the factor analysis, the proportions of the Fe^{2+} and Fe^{3+} states were obtained in each of the recorded Fe 2p spectra. The results indicate that iron was initially almost completely in the Fe^{3+} state. This is also supported by the XRD results [16] which indicate the α-Fe_2O_3 phase containing only Fe^{3+}

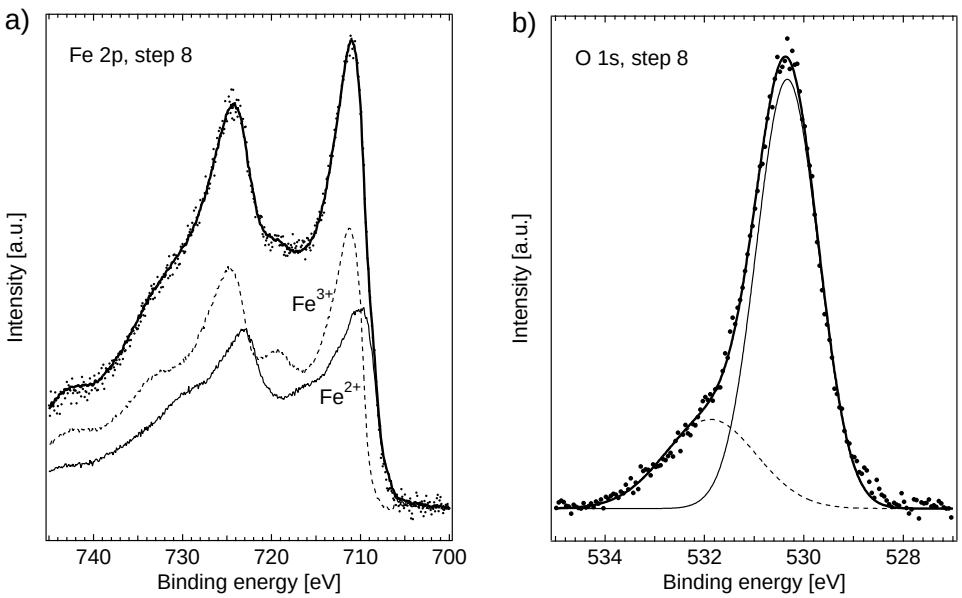

Fig. 2. a) Component spectra, Fe^{2+} (solid line) and Fe^{3+} (dashed line), obtained from the factor analysis, and a reproduction (thick solid line) of one of the Fe 2p spectra (step 8). b) One of the O 1s spectra (step 8) fitted with two Gaussian components.

cations. A small amount of Fe^{2+} was detected which could be attributed to the reducing effect of the platinum electrodes. This was confirmed by recording the Fe 2p region with the x-ray spot far from the electrodes; this produced a pure Fe^{3+} spectrum.

The broadened shape of the O 1s spectra (Fig. 1b) suggests that the oxygen is present in at least two states. Figure 2b shows a typical O 1s spectrum fitted with two Gaussian components. The main peak is located at 530.3 eV and has a FWHM of 1.5 eV. Most likely, this corresponds to O^{2-} in the iron oxide lattice. The second component is shifted by about 1.5 eV to higher binding energy and is clearly wider with a FWHM of 2.3 eV. This component could attributed to OH^- [2,6,21,24] originating possibly from H_2O used as the oxygen precursor in the film growth. The high FWHM value suggests that the second peak may also include an additional unresolved component, such as adsorbed oxygen O^- or $O_2{}^{2-}$ observed typically at about 0.7 eV and 2 eV higher than the lattice oxygen, respectively [6].

3.2 Sensor resistance

Figure 3 shows the behavior of the sensor resistance during one of the sputtering and oxygen exposure steps. Indicated in the figure is also the chemical state of iron, determined with XPS first after the sputtering and then during

the oxygen exposure. The bias voltage required to measure the sensor resistance caused broadening of the XPS spectra. In order to minimize this, the bias voltage was reduced while recording the spectra. This in turn increased noise in the resistance data as indicated by the gray areas in the figure.

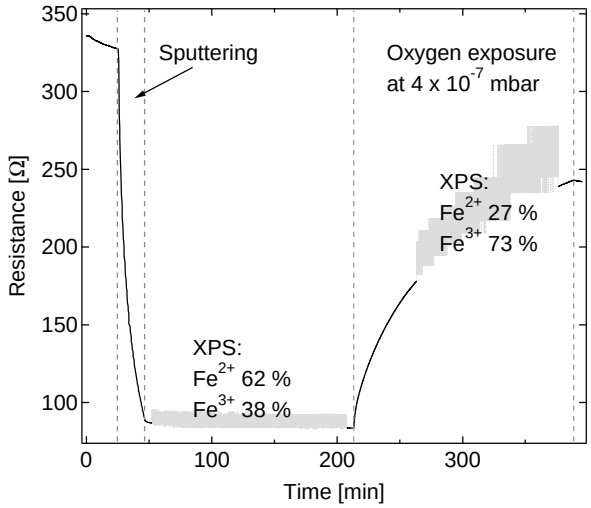

Fig. 3. Sensor resistance as a function of time along with the XPS results for the chemical state of iron in one of the treatment steps (step 13) at 300 °C. The XPS data acquisition periods are plotted in gray; the high noise level there is due to the decreased bias voltage which was used to avoid broadening of the spectra.

It is observed that the sputtering decreased the resistance rapidly from 330 Ω to 90 Ω. In each step it was ensured that the sputtering decreased the resistance below the level reached in the preceding step (here 140 Ω). In other words, the sputtering was first allowed to remove the effect of the preceding oxidation and then to set the sensor surface into a new state.

As shown in Fig. 3, the oxygen exposure increased the sensor resistance. This was accompanied with oxidation of iron which was observed with XPS as transfer of the iron intensity from the Fe^{2+} state to the Fe^{3+} state. When the exposure was stopped, the resistance started to decrease slowly. The chemical state of iron was not determined at this phase, but a possible explanation could be a slight reduction of surface iron due to transport of electrons and cations to the surface as reported by Roosendaal et al. [25].

3.3 Effects of the sputtering

The effect of the argon ion sputtering on the chemical state of iron and the sensor resistance is shown in Fig. 4a; the chemical state of iron is presented as the proportion of Fe^{2+} of the total Fe intensity. As the sputtering proceeded, the proportion of Fe^{2+} increased probably due to preferential sputtering of

oxygen over iron. In the end the surface iron had practically completely taken the Fe^{2+} state and also a small amount of metallic iron could be detected (Fig. 1a, step 17). Considering oxygen, the sputtering was found to decrease the O/Fe intensity ratio; the observed change corresponds approximately to a change in stoichiometry from Fe_2O_3 to FeO. This agrees well with the observed change in the chemical state of iron because in FeO all iron is in the Fe^{2+} state. The sputtering was also found to decrease the higher binding energy O 1s component with respect to the main component. In the last step (17) a new component with a larger shift from the main peak appeared. This could be attributed to SiO_2 of the substrate.

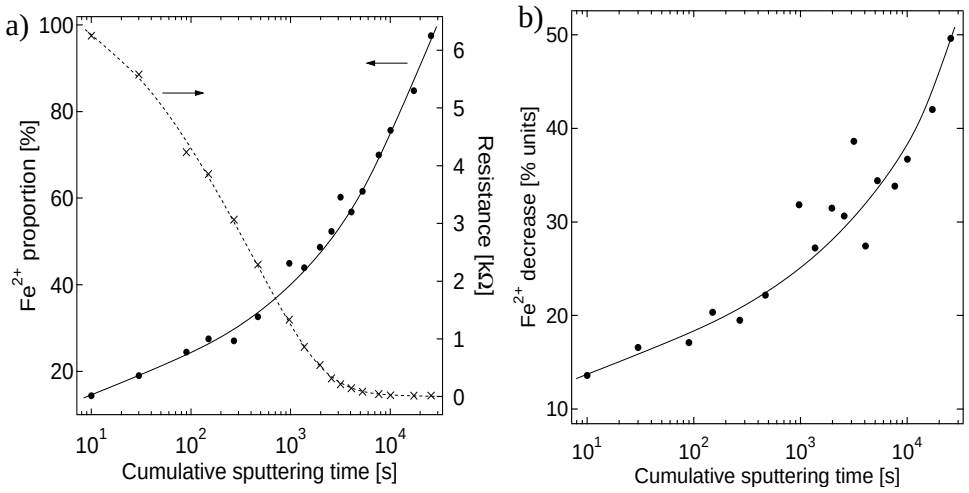

Fig. 4. a) Effect of the argon ion sputtering on the proportion of Fe^{2+} (dots, solid line) and on the sensor resistance (crosses, dashed line). b) Magnitude of iron oxidation, measured as decrease in the Fe^{2+} proportion, resulting from the oxygen exposure as a function of the cumulative sputtering time. The sputtering times are listed in detail in Table 1. Temperature of the sensor was 300 °C. The curves have been drawn to guide the eye.

Figure 4a shows that along with the reduction of iron, the sensor resistance decreased by a factor of 100 and saturated in the last few steps. Indeed, it was found in the final step that the resistance did not decrease during the sputtering anymore but started to increase. As the iron oxide was initially n-type Fe_2O_3, the decrease in the resistance as a function of the cumulative sputtering time can be first attributed to generation of oxygen vacancies which act as donors and thereby increase the density of conduction electrons. Another explanation could be enhanced electron mobility caused by the increase in the amount of Fe^{2+} ions. When the proportion of Fe^{2+} has increased substantially, the conduction behavior can be compared to Fe_3O_4 (33.3 % Fe^{2+}) and FeO (100 % Fe^{2+}) which are oxygen-excess p-type semiconductors having typically very low resistivity compared to Fe_2O_3 [11,26].

3.4 Sensitivity to oxygen

In each step, the oxygen exposure was observed to oxidize iron, increase the O 1s intensity, shift the O 1s spectrum to higher binding energy (band bending), and increase the sensor resistance. In order to quantify the oxidation of iron, the decrease in the Fe^{2+} proportion (transfer from the Fe^{2+} to Fe^{3+} state) caused by the oxygen exposure was determined from the factor analysis results. This is plotted in Fig. 4b as a function of the cumulative sputtering time. It appears that as the sputtering time increased and the iron became more reduced, the oxidation was enhanced. It should be noted that, except for the first step, the proportion of Fe^{2+} did not drop to zero, i.e. iron did not become completely oxidized to Fe^{3+}, in any of the steps.

The oxygen exposure was found to increase the O 1s intensity and decrease the relative intensity of the higher binding energy component with respect to the main peak. This indicates that the gas phase oxygen reacted with the surface and became incorporated into the iron oxide lattice. This is consistent with the observed oxidation of iron. At each step, the difference between the O 1s spectra recorded before and during the oxygen exposure was about 0.2 eV. This could be interpreted as band bending, as done by Maffeïs et al. [4], although adsorbed oxygen species, which would produce the localized surface states, could not be unambiguously detected with XPS. The assumed band bending was observed to increase during the first three steps from less than 0.05 eV to about 0.2 eV and remain then practically constant.

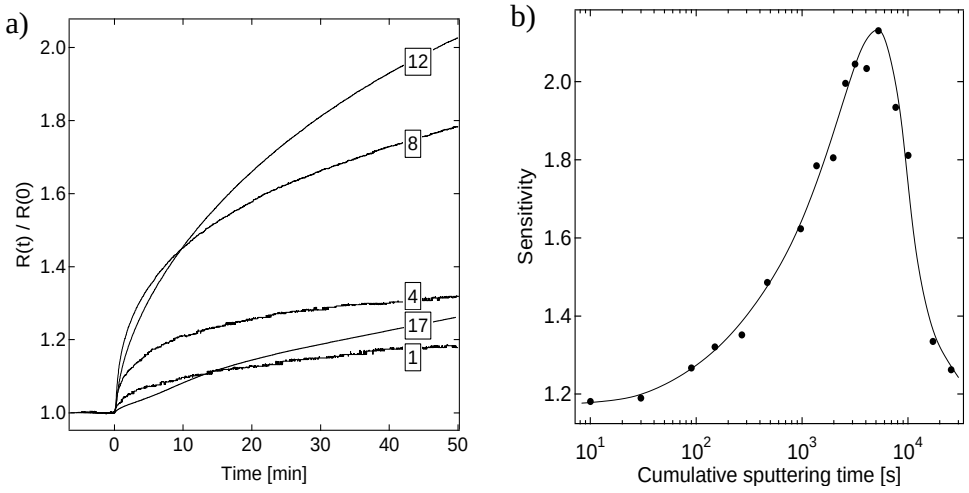

Fig. 5. a) Examples of the dynamic response of the sensor to oxygen exposure of 4×10^{-7} at 300 °C. The step index is indicated at each curve. b) Effect of the argon ion sputtering on the oxygen-sensitivity. The curve has been drawn to guide the eye.

Figure 5a shows a few examples of the resistance increase resulting from the oxygen exposure, i.e. the dynamic response of the sensor to oxygen (cf. Fig. 3).

The oxygen-sensitivity of the iron oxide film was determined from the dynamic response curves as $R(50)/R(0)$ where $R(0)$ is the sensor resistance before the oxygen exposure and $R(50)$ is the resistance in 50 minutes of exposure, just before starting the XPS data acquisition. Figure 5b represents the sensitivity as a function of the cumulative sputtering time. The figure shows that the sputtering first increased the sensitivity significantly but in the end the sensitivity collapsed back to its initial level. Figure 6 combines the observed behavior of the resistance and sensitivity as a function of chemical state of iron. It can be seen that when the Fe^{2+} proportion was less than $\sim$ 60 %, the resistance decreased and sensitivity increased as a function of the Fe^{2+} proportion. After that, the resistance saturated and sensitivity dropped significantly.

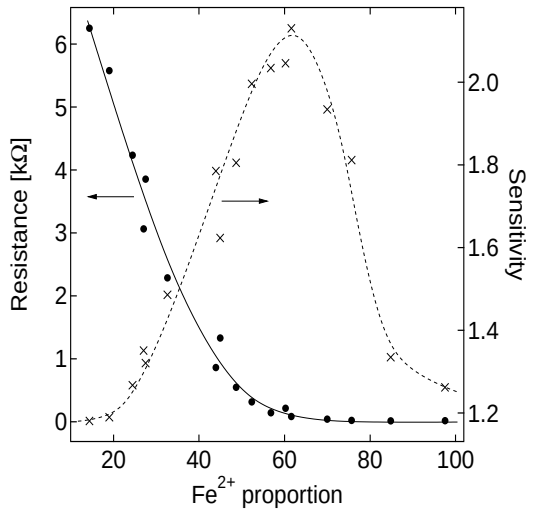

Fig. 6. Dependency of the sensor resistance and oxygen-sensitivity at 300 °C on the chemical state of iron. The curves have been drawn to guide the eye.

The results obtained before the sensitivity drop can be explained with changes in the oxygen vacancy concentration. Sputtering generates vacancies, thereby increasing the amount of conduction electrons and reducing the film resistance. The oxygen sensing takes place by oxygen filling the vacancies. As the sputtering increases the vacancy concentration, the sensitivity increases. The sensitivity drop could be attributed to enhanced p-type conduction. A p-type oxide has an oxygen excess which causes acceptor states to the band gap [1]. An oxygen exposure causes an increase in the acceptor concentration which in turn decreases the resistance. Hence, the response is the opposite compared to the n-type conductivity. As mentioned above, the conduction mechanism in those iron oxide phases that contain Fe^{2+} is p-type [11] and their resistivity is significantly lower than those containing only Fe^{3+} [26]. From this point of view it seems likely that by increasing the proportion of the Fe^{2+} state, the sputtering increased the p-type conductivity although the n-type still dominated. In addition, the shape of the dynamic response curve (Fig. 5a) seems to change with the sputtering time (becomes more linear), which

could also indicate a change in the conduction mechanism. The n–p change in the response and conduction mechanism of an iron oxide gas sensor has also been reported by Gurlo et al. [12], although there the change resulted from an inversion layer on the surface. Considering other possible explanations for the sensitivity drop, the total Fe 2p intensity was not observed to decrease in the course of sputtering. Any change was neither detected in the effect of the oxygen exposure to the O 1s spectrum, i.e. in the intensity increase and band bending. The film structures before and after the sputtering sequence were compared using AFM but no significant changes in the film morphology could be found.

Although the sensor clearly responded to oxygen, the increase in the resistance was lower than would be expected on the basis of the corresponding oxidation of iron. For example, in step 13 shown in Fig. 3, where the sensitivity is at highest, the oxygen exposure decreased the Fe^{2+} proportion to 27 % and increased the sensor resistance to about 240 Ω. For comparison, an equal proportion of Fe^{2+} measured after the sputtering produced a resistance of about 3 kΩ as can be seen around step 5 in Fig. 4a. An explanation for this difference could be that the effects of the sputtering probably extend immediately deep below the surface whereas those of the oxygen exposure take place on the surface and their depth impact is limited by the diffusion rate of, e.g., oxygen vacancies. Thus, it could be concluded that the bulk properties of the film, beyond the information depth of XPS, contribute to the resistance and that the diffusion within the lattice is slow at the used temperature (300 °C).

4 Conclusions

In this work, the correlation between the chemical state and the oxygen-sensing properties of an iron oxide thin film have been studied. The sample was subjected to a sequence of several argon ion sputtering and oxygen exposure steps and the induced changes were investigated. The sputtering was found to cause reduction of iron from the Fe^{3+} to the Fe^{2+} state and decrease the sensor resistance. In addition, the sputtering first increased the oxygen-sensitivity but in the end the sensitivity collapsed back to its initial level. The mechanism for oxygen sensing was found to be filling of the oxygen vacancies in the lattice. The effect of the sputtering on the resistance and sensitivity could be explained first with an increase in the density of oxygen vacancies and then, as the iron became more reduced, with an increase in the p-type conductivity.

Acknowledgments

The authors are grateful to Dr. M. Mäkelä (Nanoscale Oy) for the ALD growth of the iron oxide film and Mr. M. Kainlauri and Mr. T. Hyvämäki for their assistance with the resistance measurement and temperature control equipment. The work has been financially supported by the Fortum Foundation and the Academy of Finland.

References

[1] M. J. Madou, S. R. Morrison, Chemical Sensing with Solid State Devices, Academic Press, Inc., 1989.

[2] G. Gaggiotti, A. Galdikas, S. Kačiulis, G. Mattogno, A. Šetkus, Journal of Applied Physics 76 (1994) 4467.

[3] P. K. Dutta, A. Ginwalla, B. Hogg, B. R. Patton, B. Chwieroth, Z. Liang, P. Gouma, M. Mills, S. Akbar, J. Phys. Chem. B 103 (1999) 4412.

[4] T. G. G. Maffeïs, G. T. Owen, M. W. Penny, T. K. H. Starke, S. A. Clark, H. Ferkel, S. P. Wilks, Surf. Sci. 520 (2002) 29.

[5] T. G. G. Maffeïs, M. Penny, K. S. Teng, S. P. Wilks, H. S. Ferkel, G. T. Owen, Appl. Surf. Sci. 234 (2004) 82.

[6] T. Kawabe, S. Shimomura, T. Karasuda, K. Tabata, E. Suzuki, Y. Yamaguchi, Surf. Sci. 448 (2000) 101–107.

[7] C. Bittencourt, E. Llobet, M. A. P. Silva, R. Landers, L. Nieto, K. O. Vicaro, J. E. Sueiras, J. Calderer, X. Correig, Sens. Actuators B 92 (2003) 67.

[8] M. Kwoka, L. Ottaviano, M. Passacantando, S. Santucci, G. Czempik, J. Szuber, Thin Solid Films 490 (2005) 36.

[9] P. Hanyš, P. Janeček, V. Matolín, G. Korotcenkov, V. Nehasil, Surf. Sci. 600 (2006) 4233.

[10] R. F. G. Gardner, F. Sweett, D. W. Tanner, J. Phys. Chem. Solids 24 (1963) 1183.

[11] K. H. Kim, S. H. Lee, J. S. Choi, J. Phys. Chem. Solids 46 (1985) 331.

[12] A. Gurlo, M. Sahm, A. Opera, N. Barsan, U. Weimar, Sens. Actuators B 102 (2004) 291.

[13] M. Aronniemi, J. Sainio, J. Lahtinen, Surf. Sci. 601 (2007) 479.

[14] T. Suntola, Mater. Sci. Rep. 4 (1989) 261–312.

[15] M. Leskelä, M. Ritala, Thin Solid Films 409 (2002) 138–146.

[16] M. Aronniemi, J. Sainio, J. Lahtinen, Submitted to Thin Solid Films.

[17] M. Aronniemi, J. Sainio, J. Lahtinen, Surf. Sci. 578 (2005) 108.

[18] P. M. A. Sherwood, Data analysis in XPS and AES, in: D. Briggs, M. P. Seah (Eds.), Practical Surface Analysis, Volume 1, Auger and X-ray Phototoelectron Spectroscopy, 2nd Edition, John Wiley & Sons, Inc., 1990, pp. 555–586.

[19] S. Tougaard, Surf. Interface Anal. 11 (1988) 453.

[20] E. R. Malinowski, Factor Analysis in Chemistry, 2nd Edition, John Wiley & Sons, Inc., 1991.

[21] K. Wandelt, Surf. Sci. Rep. 2 (1982) 1–121.

[22] T. Fujii, F. M. F. de Groot, G. A. Sawatzky, F. C. Voogt, T. Hibma, K. Okada, Phys. Rev. B 59 (1999) 3195–3202.

[23] S. J. Roosendaal, B. van Asselen, J. W. Elsenaar, A. M. Vredenberg, F. H. P. M. Habraken, Surf. Sci. 442 (1999) 329–337.

[24] W. Lü, D. Yang, Y. Sun, Y. Guo, S. Xie, H. Li, Appl. Surf. Sci. 147 (1999) 39–43.

[25] S. J. Roosendaal, A. M. Vredenberg, F. H. P. M. Habraken, Phys. Rev. Lett. 84 (2000) 3366–3369.

[26] Y. Nakatani, M. Matsuoka, Jpn. J. Appl. Phys. 22 (1983) 233.